Journal of Systems Engineering and Electronics
Vol. 33, No. 1, February 2022, pp.38 – 46

# Feasibility of a novel beamforming algorithm via retrieving spatial harmonics

NOROLAHI Jafar [1], AZMI Paeiz [1,*], and NASIRIAN Mahdi [2]

1. Electrical and Computer Engineering Department, Tarbiat Modares University, Tehran 14115, Iran;
2. Department of Electrical and Computer Engineering, Sharif University of Technology,Tehran 11365, Iran

**Abstract:** This paper introduces an algorithm for beamforming systems by the aid of multidimensional harmonic retrieval (MHR). This algorithm resolves problems, removes limitations of sampling and provides a more robust beamformer. A new sample space is created that can be used for estimating weights of a new beamforming called spatial-harmonics retrieval beamformer (SHRB). Simulation results show that SHRB has a better performance, accuracy, and applicability and more powerful eigenvalues than conventional beamformers. A simple mathematical proof is provided. By changing the number of harmonics, as a degree of freedom that is missing in conventional beamformers, SHRB can achieve more optimal outputs without increasing the number of spatial or temporal samples. We will demonstrate that SHRB offers an improvement of 4 dB in signal to noise ratio (SNR) in bit error rate (BER) of $10^{-4}$ over conventional beamformers. In the case of direction of arrival (DOA) estimation, SHRB can estimate the DOA of the desired signal with an SNR of –25 dB, when conventional methods cannot have acceptable response.

**Keywords:** multi-input-multi-output (MIMO), beamforming, spatial and temporal signal processing, multidimensional harmonic retrieval (MHR), space-time signal processing, array signal processing.

**DOI:** 10.23919/JSEE.2022.000005

## 1. Introduction

Today, using multi-input-multi-output (MIMO) and its special applications such as beamforming has a vital role in wireless communication. Beamforming utilities have led to significant advances in spectral efficiency, user capacity, data rate, power control, power allocation, localization, beam optimization, and quality of service (QoS) in communication systems [1−8]. For example, requirement to MIMO resulted in the development of several methods in channel modelling such as Bell Labs Layered Space-Time (BLAST) and space-time coding. Thus, MIMO and beamforming are significantly noticeable in current wireless communications issues [9]. For instance, beamforming assisted networks, investigated in [10,11] for energy harvesting optimization in multi-user MIMO simultaneous wireless information and power transfer (SWIPT) systems, have low complexity and achieve near-optimal solution in both the perfect and imperfect channel state information (CSI) cases. Designing a robust beamforming in a non-convex problem to achieve minimum transmit power in SWIPT outperforms the conventional method with low complexity [12].

In practice, multidimensional harmonic retrieval (MHR) can be implemented for accurate estimation of wireless MIMO channels and beamforming [13−16]. In [16], the application of MHR to parametric channel estimation from MIMO sounding measurements is focused. It also mentions beamforming as an example of parametric channel modelling application.

In the aforementioned conditions, multipath estimation endpoints in several dimensions such as horizontal and vertical angles, delay, Doppler shift, and path loss guide us to MHR [14−16]. The number of usable dimensions depends on hypothesized mobility, Tx-Rx array geometry, sampling estimation of different dimensions as multidimensional harmonics of signals innovates a way for proper analysis of MIMO communication and special beamforming [16]. Space-time sampling in antenna array let us estimate two-dimensional harmonics or space-time harmonics [14−16].

In this paper, using spatial harmonics, we propose a novel algorithm for beamforming named spatial-harmonics retrieval beamformer (SHRB). Clear difference between conventional beamforming and SHRB is shown in this study. It benefits preprocessed sample space that is achieved by MHR. In other words, the difference between conventional beamforming and SHRB is the uti-

Manuscript received July 31, 2020.
*Corresponding author.

lity of different sample space achieved by MHR. It is also assumed that channel cannot be estimated in the temporal domain due to some limitations. The limitations can happen in situations where the signal acts as an impulse temporally or performs when a high sample-rate device is not available because of economical shortages, low space, etc. [16]. The basis of all conventional beamforming is spatial filtering on temporal samples. Thus, small temporal sampled data size can lead to low performance [17]. For example, in [17] it was emphasised that the sample matrix inversion (SMI) algorithm is not very stable in small size sampled data. Results of this study show that spatial harmonics can be well used to resolve the problems of limited sampled data in beamforming.

After spatial harmonics retrieving to provide pre-processed sampled data, SHRB uses an optimization problem (OP) such as minimum variance distortionless response (MVDR) and linearly constrained minimum variance (LCMV) to estimate the stream vector (weights vector). As a result, SHRB can be similar to a conventional beamformer in the stream vector estimating scheme, but it is absolutely different in pre-processed sampled data (see Section 4).

Conventional beamforming has two parameters as variant to optimization, temporal and spatial samples. On the contrary, SHRB by the aid of pre-processed sampled data has three parameters, temporal and spatial samples and number of harmonics as a very vital degree of freedom. In this paper, we also provide a simple mathematical proof and wide simulations to illustrate that the SHRB has better efficiency than the conventional beamforming.

The paper structure is as follows: after an introduction of SHRB in Section 1, related works are described in Section 2; data modelling and an important theorem, which is frequently applied in MHR are provided in Section 3; Section 4 comprehensively deals with a simple mathematical proof of the SHRB method, and SHRB is compared to the conventional beamformer in Section 4; Section 5 presents simulations to evaluate the performance of SHRB and the effect of harmonics number as a new degree of freedom for SHRB. We will show that this degree of freedom leads to resolution capability improvement, better retrieving of signals in temporal domain by SHRB, and better performance by better bit error rate (BER) curve versus signal to noise ratio (SNR). Also, an application of SHRB in direction of arrival (DOA) estimation is assessed. Results show that SHRB has a superior performance. Section 6 presents the conclusions.

## 2. Related works

According to [18−20], next generation 5G wireless network requires beamformer-based communications. Beamforming provides high data rates in spite of limited spectrum availability. In addition, it has further advantages for 5G wireless networks such as suppression of interferences and handling multipath effects in frequency selective channels [18−20]. In addition, designing a high-efficiency multi-functional mmWave 5G beamforming antenna system can be used to mitigate the energy efficiency problem such as battery capacity in user equipment (UE) [2]. Effective in achieving a reliable QoS, phased array usage with dual-polarized beam switching configuration was approved in [21].

Additionally, researchers consider beamforming as a useful technique for 5G wireless network [22]. The capability of MIMO smart antennas for hybrid beam forming, beam tracking, tracing, and spatial multiplexing leads to using it in 5G wireless technology [22,23]. An acceptable scheme that combines localization and beamforming was presented in [3]. It proposes a novel successive localization and beamforming scheme that uses UE location and the instantaneous channel state. Before estimation results are obtained, the beamforming vector is successively optimized. Thus, its simulation results show great performance for UE localization.

In non-orthogonal multiple access (NOMA) and mmWave communications (mmWave-NOMA), researches show that the use of beamforming in the base station (BS) and UEs and power allocation can be formulated as a nonconvex problem with triple steps solution to maximize the achievable sum rate (ASR). This Tx-Rx beamforming and power allocation can achieve significantly better performance in terms of ASR compared with conventional mmWave orthogonal multiple access systems [4].

In addition to addressing issues of beamforming mentioned above, one of the most important issues that is being researched is machine learning application in 5G. In [24], formulating the joint design of beamforming in the BS station, power control, and interference coordination as a non-convex optimization problem to maximize the signal to interference plus noise ratio (SINR) has been performed and this problem has been solved by using deep reinforcement learning. The use of beamforming in this algorithm leads to providing a dedicated beam for a given UE, through which power control and interference coordination take place, and performing power control of that beam by changing the transmit power of the BS to the UE. As a result, its algorithm approaches a better performance in terms of SINR and max sum-rate capacity. Moreover, beamforming in machine learning assisted 5G network was reported in [25−27]. Moreover, beamform-

ing has practical applications in physical layer design, and it can provide efficient power control and energy performance [28,29]. Relevant works such as angle of arrival were shown in [30−32].

In [33,34], an approach to the MHR problem is proposed based on a multi-dimensional extension of rank reduction estimator (RARE) initially developed for DOA estimation in partly calibrated arrays. Also, in [35,36], new algorithms for MHR were introduced based on iteratively reweighted tensor singular value decomposition in [13,37,38]. In this paper, we use the multidimentional embedding (MDE)-alternating least square (MDE-ALS) algorithm considered in [14] for SHRB. MDE-ALS is shown to achieve deterministic bound and remains close to Cramer-Rao bound (CRB) even at low SNRs [14].

## 3. Data modelling

In this paper, channel is modelled by two-dimensional harmonics retrieval. The noiseless two-dimensional harmonics $x_{k,l}$ is expressed as the sum of $F$ two-dimensional (2-D) exponentials shown in the following [16]:

$$x_{k,l}=\sum_{f=1}^{F}c_f\mathrm{e}^{\mathrm{j}\omega_f(k-1)}\mathrm{e}^{\mathrm{j}\nu_f(l-1)}=\sum_{f=1}^{F}c_f a_f^{k-1}b_f^{l-1} \tag{1}$$

in which, $a_f^{k-1}=\mathrm{e}^{\mathrm{j}\omega_f(k-1)}$, $b_f^{l-1}=\mathrm{e}^{\mathrm{j}\nu_f(k-1)}$, and $l=1,2,\cdots,L$ where $K$ and $L$ denote the number of samples taken along temporal and spatial dimensions respectively. Also, $\omega_f$, $\nu_f\in(-\pi,\pi)$ represent two frequencies associated with the $f$th 2-D harmonic. We must find triple parameters $(\omega_f,\nu_f,c_f)$ for $f=1,2,\cdots,F$ that $F$ is the number of harmonics and $(\omega_f,\nu_f)$ includes two frequencies which are the basis of the $f$th 2-D harmonics, where two dimensions are temporal and spatial respectively, and $c_f$ is the complex amplitudes of these 2-D harmonics.

In (1), the following definitions are used:

$$\begin{cases}\boldsymbol{X}(k,l)=x_{k,l},\ \ \boldsymbol{X}\in\mathbf{C}^{K\times L}\\ \boldsymbol{A}(k,f)=\mathrm{e}^{\mathrm{j}\omega_f(k-1)},\ \ \boldsymbol{A}\in\mathbf{C}^{K\times F}\\ \boldsymbol{B}(l,f)=\mathrm{e}^{\mathrm{j}\nu_f(l-1)},\ \ \boldsymbol{B}\in\mathbf{C}^{L\times F}.\\ \boldsymbol{C}(f,f)=c_f,\ \ \boldsymbol{C}\in\mathbf{C}^{F\times F}\end{cases}$$

In other words, matrices $\boldsymbol{A}$ and $\boldsymbol{B}$ include harmonics obtained from sampling in spatial and temporal dimensions respectively, and $\boldsymbol{C}$ is a diagonal matrix that contains harmonics amplitudes. Therefore, a mixture of the 2-D harmonics of (1) can be written in matrix form [17] as

$$\boldsymbol{X}=\boldsymbol{A}\boldsymbol{C}\boldsymbol{B}^{\mathrm{T}}. \tag{2}$$

Based on [14,15] and using Khatri-Rao multiple definitions, (2) can be shown as

$$\boldsymbol{X}=(\boldsymbol{B}\circ\boldsymbol{A})\boldsymbol{C} \tag{3}$$

where $\circ$ means Khatri-Rao (clock-wise Kronecker) procluct.

This demonstration type can be applied to the harmonic retrieval (HR) algorithm. Moreover, according to an important theorem provided in [30], if summation of $F$ undamped 2-D exponentials is as (2), for $L\geqslant 3, l=1,2,\cdots,L$ and $K\geqslant 3, k=1,2,\cdots,K$, the triple parameter $(\omega_f,\nu_f,c_f)$ is unique for $P_f(\Pi^{2F})$ $(f=1,2,\cdots,F)$ if

$$F\leqslant\left\lceil\frac{K}{2}\right\rceil\left\lceil\frac{L}{2}\right\rceil \tag{4}$$

in which $P_f(\Pi^{2F})$is a probability density function on $F$ 2-D frequencies as $f=1,2,\cdots,F$. As mentioned before, $\omega_f$ and $\nu_f$ are frequencies in spatial and temporal dimensions, respectively. Sampling limitation in temporal domain shows itself here in temporal harmonics. A more reliable beamformer will be available if we can perform optimization without leaning on temporal effects.

## 4. SHRB and conventional beamforming

The general algorithm of conventional beamforming is provided in Fig. 1(a). First, sampled array output is generally a space-time matrix $\boldsymbol{X}$, whose elements have temporal and spatial dimensions. The $K\times L$ matrix of $\boldsymbol{X}$ can be shown as follows:

$$\boldsymbol{X}=\begin{bmatrix}x_{1,1}&x_{1,2}&\cdots&x_{1,L}\\ x_{2,1}&x_{2,2}&\cdots&x_{2,L}\\ \vdots&\vdots&\ddots&\vdots\\ x_{K,1}&x_{K,2}&\cdots&x_{K,L}\end{bmatrix} \tag{5}$$

where $K$ is the number of antenna elements in array resulted from spatial sampling by array antennas, and $L$ is the number of temporal samples resulted from temporal sampling by each antenna.

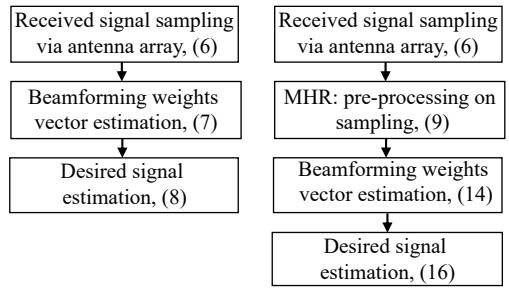


(a) Conventional beamformer algorithm (b) SHRB algorithm

**Fig. 1 Comparison of conventional beamformer and SHRB algorithms**

### 4.1 Conventional beamforming

As stated by Fig. 1(a), conventional beamforming consists of three steps in total. Step one, receiving signal or

sampling array output, is noted as

$$\boldsymbol{X} = \boldsymbol{S} + \boldsymbol{I} + \boldsymbol{N} \tag{6}$$

where $\boldsymbol{S}$ is the desired signal, $\boldsymbol{I}$ is the interference signal and $\boldsymbol{N}$ is the noise that is the assumed additive white Gaussian noise (AWGN). After receiving $\boldsymbol{X}$, in the second step we must obtain beamformer weights vector named $\bar{\boldsymbol{w}}$ from $\boldsymbol{X}$ by one of the OPs (MVDR, LCMV, etc.) [6]. The MVDR beamformer weight found by the help of the SMI algorithm is given by [14,15] as follows:

$$\bar{\boldsymbol{w}} = \widehat{\boldsymbol{R}}^{-1}\boldsymbol{a}_s \tag{7}$$

where $\boldsymbol{a}_s$ is the steering vector and $\widehat{\boldsymbol{R}}$ is the estimation of covariance matrix $\boldsymbol{R}$ of $\boldsymbol{X}$. Finally, the third step estimates the desired signal by multiplying two vectors, $\boldsymbol{X}$ and $\bar{\boldsymbol{w}}$ as

$$\widehat{\boldsymbol{S}} = \bar{\boldsymbol{w}}\boldsymbol{X} \tag{8}$$

where $\widehat{\boldsymbol{S}}$ is retrieved from the received signal $\boldsymbol{X}$. The best case of beamforming takes place when $\widehat{\boldsymbol{S}} \cong \boldsymbol{S}$.

### 4.2 SHRB

As metioned above, $\boldsymbol{X}$ elements can be shown by the 2-D HR model according to (1). Also, Fig. 1(b) shows that the proposed beamforming SHRB has four steps with one step further than conventional beamforming. The first step of SHRB is similar to the conventional beamforming, and receiving signal and sampling array output called $\boldsymbol{X}$ are performed, too. In the second step which is different from the conventional beamforming, $\boldsymbol{X}$ is changed to $\boldsymbol{X}_{\text{spatial}}$ via MHR ($M$=2, MHR is 2-D harmonics retreival in this paper). The new sampled array output, called $\boldsymbol{X}_{\text{spatial}}$, is created by the following multiplication:

$$\boldsymbol{X}_{\text{spatial}} = \widehat{\boldsymbol{A}}\,\widehat{\boldsymbol{C}}, \tag{9}$$

where $\widehat{\boldsymbol{A}}, \widehat{\boldsymbol{C}}$, and $\boldsymbol{X}_{\text{spatial}}$ can be written as

$$\widehat{\boldsymbol{A}} = \begin{bmatrix} 1 & 1 & \cdots & 1 \\ \mathrm{e}^{\mathrm{j}\omega_1} & \mathrm{e}^{\mathrm{j}\omega_2} & \cdots & \mathrm{e}^{\mathrm{j}\omega_F} \\ \mathrm{e}^{\mathrm{j}2\omega_1} & \mathrm{e}^{\mathrm{j}2\omega_2} & \cdots & \mathrm{e}^{\mathrm{j}2\omega_F} \\ \vdots & \vdots & \ddots & \vdots \\ \mathrm{e}^{\mathrm{j}(K-1)\omega_1} & \mathrm{e}^{\mathrm{j}(K-1)\omega_2} & \cdots & \mathrm{e}^{\mathrm{j}(K-1)\omega_F} \end{bmatrix}, \tag{10}$$

$$\widehat{\boldsymbol{C}} = \begin{bmatrix} c_1 & 0 & \cdots & 0 \\ 0 & c_2 & \cdots & 0 \\ \vdots & \vdots & \ddots & \vdots \\ 0 & 0 & \cdots & c_F \end{bmatrix}_{F\times F}, \tag{11}$$

$$\boldsymbol{X}_{\text{spatial}} = \begin{bmatrix} x_{1,1} & x_{1,2} & \cdots & x_{1,F} \\ x_{2,1} & x_{2,2} & \cdots & x_{2,F} \\ \vdots & \vdots & \ddots & \vdots \\ x_{K,1} & x_{K,2} & \cdots & x_{K,F} \end{bmatrix}_{K\times F}. \tag{12}$$

It achieves isolated data from the temporal sampling limitation described in (9), because $\boldsymbol{X}_{\text{spatial}}$ only contains spatial harmoics. Actually, $\boldsymbol{X}_{\text{spatial}}$ is provided by estimation of spatial harmonics. For more clearance, according to (2), MHR obtains three submatrices of $\boldsymbol{X}$ named $\widehat{\boldsymbol{A}}$, $\widehat{\boldsymbol{B}}$, and $\widehat{\boldsymbol{C}}$. Here, $\widehat{\boldsymbol{A}}$ and $\widehat{\boldsymbol{B}}$ are Vandermond matrices, as $\widehat{\boldsymbol{A}}$ includes spatial harmonics and $\widehat{\boldsymbol{B}}$ includes temporal harmonics. Also, $\widehat{\boldsymbol{C}}$ is a diagonal matrix including the amplitudes of the harmonics.

It should be noted that $\boldsymbol{X}_{\text{spatial}}$ in (9) is not the estimation of the desired signal. It is a pre-processed version of the received signal $\boldsymbol{X}$ (see Fig. 1(b)). Now, after implementation of 2-D-HR, according to (9)−(12), each element of $\boldsymbol{X}_{\text{spatial}}$ can be written as

$$\boldsymbol{X}_{\text{spatial}_k} = \sum_{f=1}^{F} c_f \mathrm{e}^{\mathrm{j}\omega_f(k-1)} \tag{13}$$

where, similar to (1), $k = 1, 2, \cdots, K$ and $K$ denotes the number of samples that is taken along spatial dimension by the antennas, and $f = 1, 2, \cdots, F$ and $F$ is the number of harmonics. Moreover, $\omega_f \in (-\pi, \pi)$ contains the frequency associated with the $f$th spatial harmonic (spatial harmonic number $f$). In addition, the third step of SHRB is similar to the conventional beamforming algorithm. It obtains beamformer weights vector $\bar{\boldsymbol{w}}_{\text{SHRB}}$ via an OP (MVDR, LCMV, etc.). For example, the MVDR problem gives $\bar{\boldsymbol{w}}_{\text{SHRB}}$ as follows:

$$\bar{\boldsymbol{w}}_{\text{SHRB}} = \widehat{\boldsymbol{R}}_{\text{spatial}}^{-1}\boldsymbol{a}_s \tag{14}$$

where $\boldsymbol{a}_s$ is the steering vector and $\widehat{\boldsymbol{R}}_{\text{spatial}}$ is the estimation of the covariance matrix of $\boldsymbol{X}_{\text{spatial}}$, which is equal to

$$\widehat{\boldsymbol{R}}_{\text{spatial}} = \mathrm{E}\left\{\boldsymbol{X}_{\text{spatial}}\boldsymbol{X}_{\text{spatial}}^{\mathrm{H}}\right\}. \tag{15}$$

Finally, in the forth step of SHRB, the desired signal $\widehat{\boldsymbol{S}}$ is extracted by an equation that is completely similar to (8), however, it uses $\bar{\boldsymbol{w}}_{\text{SHRB}}$ instead of $\bar{\boldsymbol{w}}$. Thus, the desired signal is recovered by

$$\widehat{\boldsymbol{S}} = \bar{\boldsymbol{w}}_{\text{SHRB}}\boldsymbol{X}. \tag{16}$$

The comparison between (7) and (14) shows that the difference of conventional and SHRB algorithms is the difference between $\boldsymbol{X}$ and $\boldsymbol{X}_{\text{spatial}}$ which leads to more efficient beamformer in SHRB. More efficiency of SHRB pertains to its new degree of freedom, or the number of harmonics $F$ (see Fig. 1(b)).

### 4.3 Mathematical proof of SHRB

In reality, the interference covariance matrix is not known and must be estimated from some training data. To estimate $\widehat{\boldsymbol{R}}_{\text{saptial}}$ in (15) we should use a standard assumption that there exists a set of homogeneous training data that consist of independent samples data components or snap-

shots. Using these training data, the maximum likelihood (ML) estimate of $\widehat{\boldsymbol{R}}_{\text{saptial}}$ can be calculated. If training data is

$$\boldsymbol{Z}=\left[\begin{array}{c} z_{\text{spatial}_1} \\ \\ z_{\text{spatial}_N} \end{array}\right] \tag{17}$$

where $N=KF$, the ML estimate of the covariance matrix [39,40] is

$$\widehat{\boldsymbol{R}}_{\text{spatial}}=\frac{1}{M}\boldsymbol{Z}_{\text{spatial}}\boldsymbol{Z}_{\text{spatial}}^{\text{H}}=\frac{1}{M}\sum_{m=1}^{M}\boldsymbol{Z}_{\text{spatial}}(m)\boldsymbol{Z}_{\text{spatial}}^{\text{H}}(m) \tag{18}$$

where $M$ is the number of snapshots. This is called the SMI algorithm which is an asymptotically good estimate. For a small sample size, it is known to be not very stable [15]. According to Brennan's rule [16], If one wishes to maintain an average loss less than 3 dB, at least $M=2N$. In other words, for SHRB, the following condition should be satisfied:

$$M\geqslant 2N \tag{19}$$

where $N=KF$. Thus the new degree of freedom rule is more distinguished here. In case of limitation in sampling in one dimension, it can act as a dimension completely. It means, beamformer does not need to increase samples in a dimension to compensate another dimension sampling limitation. For example, increasing $F$ can compensate low temporal sample size and SHRB does not need to increase the number of sensors in array $K$. Here, the mathematical proof of SHRB superiority is completed.

### 4.4 SHRB complexity

According to Fig. 1, SHRB has one more step—MHR implementation—than conventional beamformer. Thus, compared with conventional beamformer, its complexity of actual implementation is closely related to MHR complexity. The complexity of MHR is evaluated in [13,34,37,38]. As a result, the complexity of SHRB is linear with respect to the number of measurements, which allows processing of large size signals.

The most expensive step is the initial pre-processing step, which has a complexity of the size of

$$6\left(\prod_{d=1}^{d}\boldsymbol{I}_d\right)M^2$$

where $M$ is the number of snapshots, and $\boldsymbol{I}_d$ and $d$ are the identity matrix and the number of harmonics dimensions (in this study $d=2$). Additionally, the computation of the matrices in (2) used in the construction of $\boldsymbol{X}=\boldsymbol{ACB}^{\text{T}}$, with a complexity of the order of

$$2d\left(\prod_{d=1}^{d}I_d\right)R^2$$

where $R=KL$ is the number of $\boldsymbol{X}$ entries.
The total complexity is of the order of

$$\left(6M+4\frac{(KL)^2}{M}\right)\left(\prod_{d=1}^{2}\boldsymbol{I}_d\right)M^2.$$

If there are many snapshots and temporal sampling $M\gg K$, then the complexity is relational by $M^3$. In addition, if $M\ll R$, it means we have limitation in snapshots and temporal sampling. Thus, the complexity is relational by $K^2$.

In Table 1, the computational complexities of SHRB and some conventional beamforming algorithms such as MVDR and multiple signal classifier (MUSIC) are compared [17]. As a result, SHRB complexity in low snapshots is similar to conventional algorithms such as MVDR, and SHRB takes more computational complexity in many snapshots because of estimating the construction of $\boldsymbol{X}=\boldsymbol{ACB}^{\text{T}}$.

**Table 1 Computational complexities of SHRB and conventional algorithms**

| Algorithm | Computational complexity | Low signal sample number | High signal sample number |
|---|---|---|---|
| SHRB | $\left(6M+4\frac{(KL)^2}{M}\right)\left(\prod_{d=1}^{2}\boldsymbol{I}_d\right)M^2$ | $K^2$ | $M^3$ |
| MVDR | $K^2(M+6)+M+4$ | $K^2$ | $2M$ |
| MUSIC | $\frac{5}{3}K^3+K^2(M+K+2)+4$ | $\frac{8}{3}K^3$ | $M$ |

## 5. Evaluation of SHRB performance and simulation

In the following subsections, comparisons between the conventional beamforming and SHRB are performed.

### 5.1 New degree of freedom in SHRB

In this subsection, the following scenario is simulated to prove that the number of harmonics can be a degree of freedom in SHRB:

(i) Desired signal DOA: 45° horizontal and 0° vertical;
(ii) Interference 1 DOA: 20° horizontal and 0° vertical;
(iii) Interference 2 DOA: 60° horizontal and 0° vertical;
(iv) SINR = −14 dB;
(v) Temporal samples number = 76;
(vi) Spatial samples = 56;
(vii) Harmonics number can be variable;
(viii) Physical channel is assumed as Rician fading channel with AWGN.

#### 5.1.1 Evaluating the effect of harmonics number

The effect of harmonics number in beamformer is evaluated in this section. Fig. 2 shows the result of interfe-

rences suppression in SHRB for 150 and 190 harmonics compared with the conventional beamformer. Red solid and black dashed curves denote SHRB results for 190 and 150 harmonics, respectively, and green circles denote the conventional result. If we define accuracy as capability of finding and recognizing interferences from the desired signal, then results illustrate that the accuracy and nulls depth of SHRB results are more proper than the conventional beamformer. Thus, the SHRB performance is better. In case of interferences suppression, the difference between SHRB and conventional beamformer appears because of an additional degree of freedom as number of harmonics that can be adjusted to obtain better results. Besides, Fig. 2 shows that 190 harmonics provide deeper null than 150 harmonics.

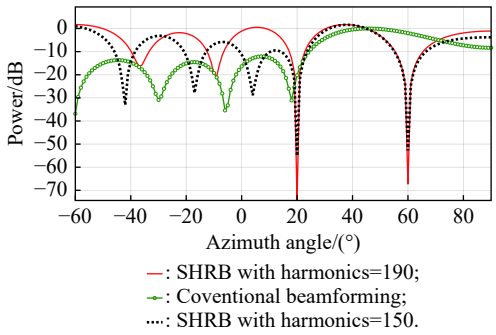


**Fig. 2 Evaluation of the effect of harmonics number (elevation angle = 0°)**

Moreover, outcomes of eigenvalues estimation for $\boldsymbol{X}$ and $\boldsymbol{X}_{\text{spatial}}$ in Fig. 3(a) and Fig. 3(b) verify the results of Fig.2, because $\boldsymbol{X}_{\text{spatial}}$ eigenvalues in 190 and 150 harmonics have larger amplitudes than $\boldsymbol{X}$ ones. Regarding the simulation results, SHRB performs more accurately than the conventional beamformer. It has deep nulls in the DOAs of the interferences, while the conventional beamformer does not have such nulls. Furthermore, it can be said that the number of harmonics plays an important role for improving SHRB performance.

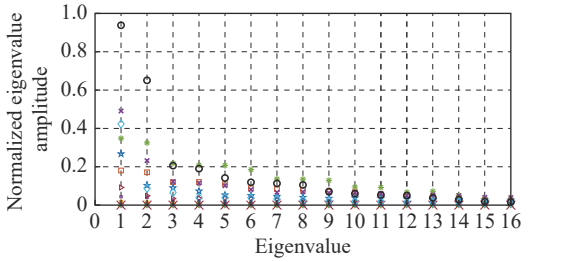


(a) $\boldsymbol{X}_{\text{spatial}}$ eigenvalue amplitudes by harmonics number

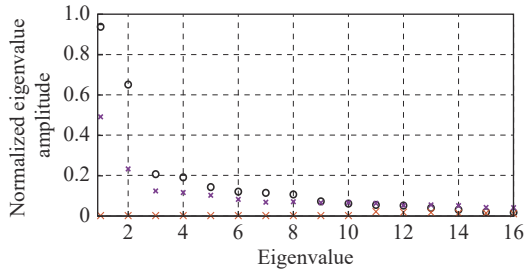


: Preprocessed signal, $\boldsymbol{X}_{\text{spatial}}$ eigenvalues for 190 harmonics;
: Preprocessed signal, $\boldsymbol{X}_{\text{spatial}}$ eigenvalues for 150 harmonics;
: Received signal, $\boldsymbol{X}$ eigenvalues.

(b) Comparison of $\boldsymbol{X}_{\text{spatial}}$ and $\boldsymbol{X}$ eigenvalue amplitudes

**Fig. 3 Eigenvalues estimation**

### 5.1.2 Resolution capability improvement

In this paper, resolution means the ability to resolve interferences with very near DOAs. Fig. 4 shows a resolution of 1° case for the following simulated situation:

(i) Desired signal DOA: 31° horizontal and 0° vertical
(ii) Interference 1 DOA: 30° horizontal and 0° vertical
(iii) Interference 2 DOA: 32° horizontal and 0° vertical

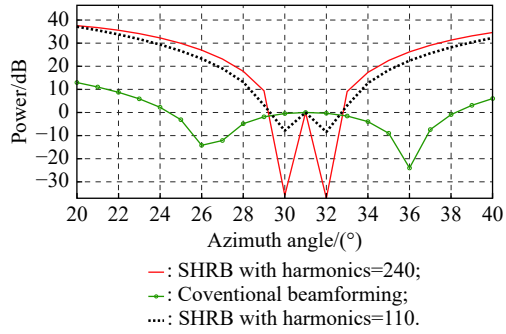


**Fig. 4 Resolution capability of SHRB and conventional beamformer**

In Fig.4, red solid and black dashed curves denote the SHRB results for 190 and 150 harmonics respectively and the green circle denotes the conventional result. The comparison shows that, in contrast to the unacceptable response of the conventional beamformer (due to wrong estimation in desired DOAs), SHRB has nulls in the DOAs of the interferences. Results indicate that increasing the number of harmonics in the scope of (4) leads to deeper nulls in DOAs of interference signals and does not cause any null or amplification in DOA of desired signals. On the other hand, as the conventional beamformer is not dependent on the harmonics in its structure, its results do not change with increasing the number of harmonics. Therefore, SHRB leads to better results in resolution. It

occurs for at least two reasons. First, the SHRB algorithm can overcome the temporal sampling limitation by preprocessing of (9). Second, it has an additional degree of freedom as the number of harmonics which can improve the SHRB results and does not exist in the conventional beamforming.

### 5.2 Signal reconstruction and retrieving in time domain by SHRB

In this part of the article, signal reconstruction in time domain is presented. The desired signal is a pulse with SNR equal to −5 dB. The results are shown in Fig. 5. Red solid and black dashed curves denote SHRB results for 190 and 150 harmonics respectively and the green circle denotes the result of the conventional beamforming. As is seen, signal reconstruction in the time domain with the conventional beamforming is not acceptable, while SHRB is completely successful.

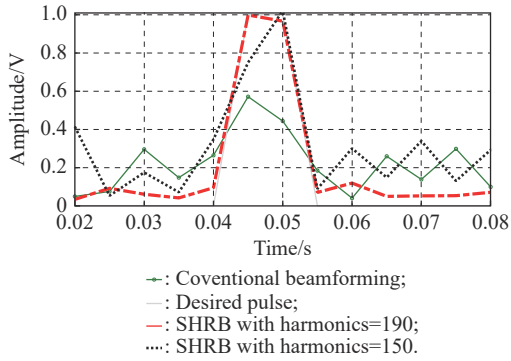


**Fig. 5 Reconstruction and retrieving of signal in time domain for SNR= −5 dB**

Again, as an example of the effect of the novel degree of freedom for SHRB, by increasing the harmonics number from 150 to 190, shape of the retrieved pulse in time domain in SHRB output has become more accurate, while the result is not changeable in the conventional beamforming, unless the number of the array antennas or temporal samples is increased. This means that SHRB adequately retrieves the desired signal since it resolves the limitations of temporal samplings by preprocessing indicated in (9).

### 5.3 Comparison of BERs

In this subsection, BER evaluation is provided. Fig. 6 indicates the BERs of SHRB and the conventional beamformer versus SNR in the same conditions (same number of spatial and temporal samples). The red dashed curve belongs to the conventional beamforming and the blue circle curve is SHRB BER. According to Fig. 6, it is clear that SHRB has a better performance than the conventional beamformer, because its BER curve has 3 dB and 4 dB SNR advantages in BER=$10^{-2}$ and BER=$10^{-4}$ respectively over the conventional beamforming. Therefore, it can be said that the BER is improved by the SHRB assistance because it benefits desired signal retrieving more accurately. Fig. 6 absolutely shows the superiority, robustness, and reliability of SHRB.

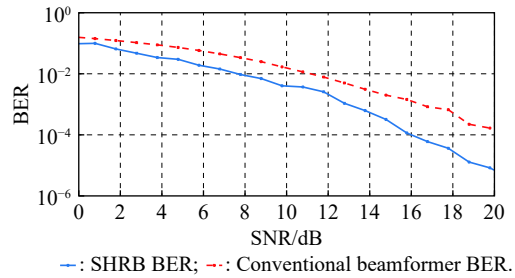


**Fig. 6 BER of SHRB and conventional beamformer versus SNR**

### 5.4 DOA estimation by the aid of SHRB

Because of its reliable results, SHRB can be used in some applications such as DOA estimation. There are two signal sources in DOAs: (37° azimuth, 23° elevation) and (−45° azimuth, 4° elevation) that must be detected by both SHRB and the conventional algorithms with SNR= −25 dB.

Fig. 7 presents the results that corroborate the high-resolution performance of localization and DOA estimating by SHRB. As can be seen in Fig. 7, the conventional algorithm does not have any acceptable estimation of DOAs in SNR=−25 dB because it is out of conventional DOA estimator SNR range. Moreover, SHRB assisted DOA estimator can estimate DOA of the desired signal. As mentioned in Section 3.3, SHRB does not need to increase samples in a dimension to compensate another dimension sampling limitation. For example, increasing $F$ can compensate the small temporal sample size, and it does not need to increase the number of sensors in array $K$. Thus, the SHRB, preprocessing indicated in (9) and resolving temporal sampling by new degree of freedom, is able to obtain more efficient DOA estimating.

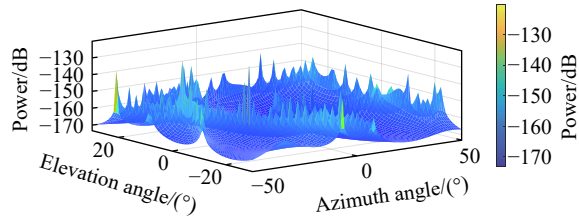


(a) Conventional beamforming

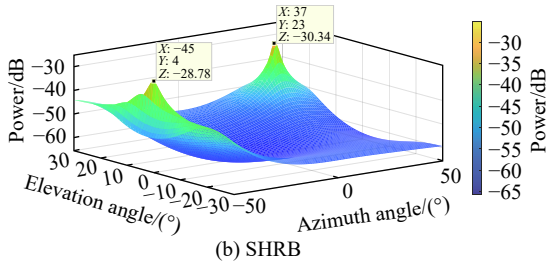


(b) SHRB

**Fig. 7 DOA estimation**

## 6. Conclusions

In this paper, a novel algorithm for beamforming called SHRB is introduced. According to the results, SHRB leads to improvements in accuracy, robustness, and reliability, with respect to the conventional beamforming. It isolates the sample space from its temporal limitations by MHR, to mitigate temporal limitations described in Section 3. Since SHRB uses the number of harmonics as a new degree of freedom, it can provide better results without need for increasing the number of temporal samples or the number of array sensors and only by increasing the number of harmonics. This degree of freedom is not accessible in the conventional beamforming. Simple mathematical proof is presented in Section 3. In order to confirm the SHRB advantages, we first illustrate the effectiveness of the new degree of freedom (number of harmonics), resolution accuracy, BER, temporal retrieving of signal, and then, an application of SHRB, DOA estimation. For all of these features, results have been compared with the conventional beamforming. For example, BER curve of SHRB has a 3 dB SNR advantage in BER=$10^{-2}$ and a 4 dB SNR advantage in BER=$10^{-4}$ over the conventional beamforming. This proves the superiority, robustness and reliability of SHRB. In addition, it has acceptable DOA estimation results in SNR = −25 dB, while the conventional algorithm does not have acceptable results.

## References

[1] DONG M, WANG Q Q. Multi-group multicast beamforming: optimal structure and efficient algorithms. IEEE Trans. on Signal Processing, 2020, 68: 3738–3753.

[2] PARK J, SEONG H, WHANG Y N, et al. Energy-efficient 5G phased arrays incorporating vertically polarized endfire planar folded slot antenna for mmWave mobile terminals. IEEE Trans. on Antennas and Propagation, 2020, 68(1): 230–241.

[3] ZHOU B P, LIU A, LAU V. Successive localization and beamforming in 5G mmWave MIMO communication systems. IEEE Trans. on Signal Processing, 2019, 67(6): 1620–1635.

[4] ZHU L P, ZHANG J, XIAO Z Y, et al. Joint Tx-Rx beamforming and power allocation for 5G millimeter-wave non-orthogonal multiple access networks. IEEE Trans. on Communications, 2019, 67(7): 5114–5125.

[5] HO K C, TSAI S H. A novel multiuser beamforming system with reduced complexity and beam optimizations. IEEE Trans. on Wireless Communications, 2019, 18(9): 4544–4557.

[6] FOSCHINI G J, GANS M J. On limits of wireless communications in a fading environment when using multiple antennas. Wireless Personal Communications, 1998, 6(3): 311–335.

[7] NIKBAKHT R, MOSAYEBI R, LOZANO A. Uplink fractional power control and downlink power allocation for cell-free networks. IEEE Wireless Communications Letters, 2020, 9(6): 774–777.

[8] ASIEDU D K P, MAHAMA S, SONG C, et al. Beamforming and resource allocation for multiuser full-duplex wireless-powered communications in IoT networks. IEEE Internet of Things Journal, 2020, 7(12): 11355–11370.

[9] PEHLIVAN I, ERGEN S C. Scheduling of energy harvesting for MIMO wireless powered communication networks. IEEE Communications Letters, 2019, 23(1): 152–155.

[10] JU M, YANG H C. Rate-energy outage analysis of MISO SWIPT with multiple energy harvesting sensors. IEEE Access, 2019, 7: 177187–177197.

[11] XU K, SHEN Z X, ZHANG M, et al. Beam-domain SWIPT for mMIMO system with nonlinear energy harvesting legitimate terminals and a non-cooperative terminal. IEEE Trans. on Green Communications and Networking, 2019, 3(3): 703–720.

[12] ZHU Z Y, CHU Z, WANG Z Y, et al. Outage constrained robust beamforming for secure broadcasting systems with energy harvesting. IEEE Trans. on Wireless Communications, 2016, 15(11): 7610–7620.

[13] SORENSEN M, DE LATHAUWER L. Multidimensional harmonic retrieval via coupled canonical polyadic decomposition —part II: algorithm and multirate sampling. IEEE Trans. on Signal Processing, 2017, 65(2): 528–539.

[14] LIU X Q, SIDIROPOULOUS N D, SWAMI A. Blind high-resolution localization and tracking of multiple frequency hopped signals. IEEE Trans. on Signal Processing, 2002, 50(4): 889–901.

[15] JIANG T, SIDIROPOULOUS N D, TEN BERGE J M F. Almost-sure identifiability of multidimensional harmonic retrieval. IEEE Trans. on Signal Processing, 2001, 49(9): 1849–1859.

[16] LIU X Q, SIDIROPOULOS N D, JIANG T. Multidimensional harmonic retrieval with applications in MIMO wireless channel sounding. GERSHMAN A B, SIDIROPOULOS N D, ed. Space-time processing for MIMO communications. West Sussex: John Wiley & Sons Ltd, 2005: 41–74.

[17] NICKEL U. Principles of adaptive array processing. Advanced Radar Systems, Signal and Data Processing, 2006, 5: 1-1–1-20.

[18] REZAEI A, AZMI P, YAMCHI N M, et al. Robust resource allocation for cooperative MISO-NOMA-based heterogeneous networks. IEEE Trans. on Communications, 2021, 69(6): 3864–3878.

[19] ZHANG R Q, ZHOU J Y, YANG B Q, et al. A high-precision hybrid analog and digital beamforming transceiver system for 5G millimeter-wave communication. IEEE Access, 2019, 7: 83012–83023.

[20] LI Y-N R, GAO B, ZHANG X D, et al. Beam management in millimeter-wave communications for 5G and beyond. IEEE Access, 2020, 8: 13282–13293.
[21] HONG W B, BAEK K H, KO S. Millimeter-wave 5G antennas for smartphones: overview and experimental demonstration. IEEE Trans. on Antennas and Propagation, 2017, 65(12): 6250–6261.
[22] CHETTRI L, BERA R. A comprehensive survey on Internet of Things (IoT) toward 5G wireless systems. IEEE Internet of Things Journal, 2020, 7(1): 16–32.
[23] AKPAKWU G A, SILVA B J, HANCKE G P, et al. A survey on 5G networks for the Internet of Things: communication technologies and challenge. IEEE Access, 2018, 6: 3619–3647.
[24] MISMAR F B, EVANS B L, ALKHATEEB A. Deep reinforcement learning for 5G networks: joint beamforming, power control, and interference coordination. IEEE Trans. on Communications, 2020, 68(3): 1581–15920.
[25] ZHU L P, ZHANG J, XIAO Z Y, et al. Joint power control and beamforming for uplink non-orthogonal multiple access in 5G millimeter-wave communications. IEEE Trans. on Wireless Communications, 2018, 17(9): 6177−6189.
[26] BOGALE T E, WANG X B, LE L B. Adaptive channel prediction, beamforming and scheduling design for 5G V2I network: analytical and machine learning approaches. IEEE Trans. on Vehicular Technology, 2020, 69(5): 5055–5067.
[27] HUO Y M, DONG X D, XU W, et al. Enabling multi-functional 5G and beyond user equipment: a survey and tutorial. IEEE Access, 2019, 7: 116975–117008.
[28] HUU P, ARFAOUI M A, SHARAFEDDINE S, et al. A low-complexity framework for joint user pairing and power control for cooperative NOMA in 5G and beyond cellular networks. IEEE Trans. on Communications, 2020, 68(11): 6737–6749.
[29] JEE J, KWON G, PARK H. Precoding design and power control for SINR maximization of MISO system with nonlinear power amplifiers. IEEE Trans. on Vehicular Technology, 2020, 69(11): 14019–14024.
[30] MATSKANI E, SIDIROPOULOS N D, LUO Z Q, et al. Efficient batch and adaptive approximation algorithms for joint multicast beamforming and admission control. IEEE Trans. on Signal Processing, 2009, 57(2): 4882−4894.
[31] ZHOU X, CHEN L, YAN J, et al. Accurate DOA estimation with adjacent angle power difference for indoor localization. IEEE Access, 2020, 8: 44702–44713.
[32] ABOHAMRA Y A, SOLEYMANI M R, SHAYAN Y R. Using beamforming for dense frequency reuse in 5G. IEEE Access, 2019, 7: 9181–9190.
[33] PESAVENTO M, MECKLENBRAUKER C F, BOHME J F. Multi-dimensional harmonic estimation using K-D RARE in application to MIMO channel estimation. Proc. of the IEEE International Conference on Acoustics, Speech, and Signal Processing, 2003: DOI: 10.1109/ICASSP.2003.1202725.
[34] NION D, SIDIROPOULUS N D. Tensor algebra and multi-dimensional harmonic retrieval in signal processing for MIMO radar. IEEE Trans. on Signal Processing, 2010, 58(11): 5693–5705.
[35] WEN F X, SO C H. Robust multi-dimensional harmonic retrieval using iteratively reweighted HOSVD. IEEE Signal Processing Letters, 2015, 22(12): 2464–2468.
[36] SUN W Z, LIN X, SO H C, et al. Iteratively reweighted tensor SVD for robust multi-dimensional harmonic retrieval. Proc. of the IEEE International Conference on Acoustics, Speech and Signal Processing, 2016: 4318–4322.
[37] LIN C H, FANG W H. Efficient multidimensional harmonic retrieval: a hierarchical signal separation framework. IEEE Signal Processing Letters, 2013, 20(5): 427–430.
[38] SORENSEN M, DE LATHAUWER L. Multidimensional harmonic retrieval via coupled canonical polyadic decomposition—part I: model and identifiability. IEEE Trans. on Signal Processing, 2017, 65(2): 517–527.
[39] REED I S, MALLETT J D, BRENNAN L E. Rapid convergence rate in adaptive arrays. IEEE Trans. on Aerospace and Electronic Systems, 1974, AES-10(6): 853–863.
[40] LIU J, LIU W J, LIU H W. A simpler proof of rapid convergence rate in adaptive arrays. IEEE Trans. on Aerospace and Electronic Systems, 2017, 53(1): 135–136.

## Biographies

**NOROLAHI Jafar** was born in 1985. He received his M.S. degree in communication engineering from Tarbiat Modares University, Tehran, Iran, in 2015. He was awarded the Top Student Prize in Communication Field at Tarbiat Modares University in 2015. Since 2012, he has been with the telecommunication research center in Tehran in a researcher position. His current research focus is machine learning implementation in 5G cellular network technology. His research interests include wireless communications, signal processing, antenna array, MIMO, and machine learning.
E-mail: j.narlahi@gmail.com

**AZMI Paeiz** was born in 1974. He received his B.S., M.S., and Ph.D. degrees in electrical engineering from Sharif University of Technology (SUT), Tehran, Iran, in 1996, 1998, and 2002, respectively. Since September 2002, he has been with the Electrical and Computer Engineering Department of Tarbiat Modares University, where he became an associate professor in 2006 and he is a full professor now. From 1999 to 2001, he was with the Advanced Communication Science Research Laboratory, Iran Telecommunication Research Center (ITRC), Tehran, Iran. From 2002 to 2005, he was with the Signal Processing Research Group at ITRC. He is a senior member of IEEE. His current research interests include modulation and coding techniques, digital signal processing, wireless communications, resource allocation, molecular communications, and estimation and detection theories.
E-mail: pazmi@modares.ac.ir

**NASIRIAN Mahdi** was born in 1988. He received his B.S. degree from University of Tehran, Tehran, Iran, in 2003, and his M.S. and Ph.D. degrees in electrical engineering from Sharif University of Technology (SUT), Tehran, Iran, in 2005 and 2013 respectively. His research interests include digital signal processing with application to communication systems, radar design, and synthetic aperture radar.
E-mail: m.nasirian@alum.sharif.edu